

Optical follow-up observations of PTF10qts, a luminous broad-lined Type Ic supernova found by the Palomar Transient Factory

E. S. Walker,^{1,2★} P. A. Mazzali,^{3,4,5} E. Pian,^{1,6,7} K. Hurley,⁸ I. Arcavi,⁹
S. B. Cenko,^{10,11} A. Gal-Yam,⁹ A. Horesh,¹² M. Kasliwal,^{13†} D. Poznanski,¹⁴
J. M. Silverman,^{15‡} M. Sullivan,¹⁶ J. S. Bloom,¹¹ A. V. Filippenko,¹¹ S. R. Kulkarni,¹²
P. E. Nugent,^{11,17} E. Ofek,⁹ S. Barthelmy,¹⁰ W. Boynton,¹⁸ J. Goldsten,¹⁹
S. Golenetskii,²⁰ M. Ohno,²¹ M. S. Tashiro,²² K. Yamaoka²³ and X. L.-. Zhang²⁴

¹Scuola Normale Superiore di Pisa, Piazza dei Cavalieri 7, I-56126 Pisa, Italy

²Yale University, Department of Physics, PO Box 208120, New Haven, CT 06520-8120, USA

³Astrophysics Research Institute, Liverpool John Moores University, Liverpool Science Park, IC2 Building, 146, Brownlow Hill, Liverpool L3 5RF, UK

⁴INAF-Padova Astronomical Observatory, Vicolo dell'Osservatorio 5, I-35122 Padova, Italy

⁵Max Planck Institute for Astrophysics, Garching, Karl-Schwarzschild-Str. 1, Postfach 1317, D-85741 Garching, Germany

⁶INAF-IASF, Via P. Gobetti 101, I-40129 Bologna, Italy

⁷INFN, Sezione di Pisa, Largo Pontecorvo 3, I-56127 Pisa, Italy

⁸U.C. Berkeley Space Sciences Laboratory, 7 Gauss Way, Berkeley, CA 94720-7450, USA

⁹Department of Particle Physics and Astrophysics, The Weizmann Institute of Science, Rehovot 76100, Israel

¹⁰NASA Goddard Space Flight Center, Mail Code 661, Greenbelt, MD 20771, USA

¹¹Department of Astronomy, University of California, Berkeley, CA 94720-3411, USA

¹²Cahill Center for Astrophysics, California Institute of Technology, Pasadena, CA 91125, USA

¹³Carnegie/Princeton Fellow, 813 Santa Barbara St, Pasadena, CA 91101, USA

¹⁴School of Physics and Astronomy, Tel-Aviv University, Tel-Aviv 69978, Israel

¹⁵Department of Astronomy, University of Texas at Austin, Austin, TX 78712, USA

¹⁶School of Physics and Astronomy, University of Southampton, Southampton, SO17 1BJ, UK

¹⁷Lawrence Berkeley National Laboratory, 1 Cyclotron Road, Berkeley, CA 94720, USA

¹⁸University of Arizona, Lunar and Planetary Laboratory, Tucson, AZ 85721, U.S.A.

¹⁹Applied Physics Laboratory, Johns Hopkins University, Laurel, MD 20723, U.S.A.

²⁰Ioffe Physico-Technical Institute of the Russian Academy of Sciences, St. Petersburg, 194021, Russian Federation

²¹Department of Physical Science, Hiroshima University, 1-3-1 Kagamiyama, Higashi-Hiroshima, Hiroshima 739-8526, Japan

²²Department of Physics, Saitama University, 255 Shimo-Okubo, Sakura-ku, Saitama 338-8570, Japan

²³Department of Physics and Mathematics, Aoyama Gakuin University, 5-10-1 Fuchinobe, Sagamihara, Kanagawa 229-8558, Japan

²⁴Max-Planck-Institut für extraterrestrische Physik, Giessenbachstrasse, Garching, 85748 Germany

Accepted 2014 May 19. Received 2014 May 19; in original form 2014 March 10

ABSTRACT

We present optical photometry and spectroscopy of the broad-lined Type Ic supernova (SN Ic-BL) PTF10qts, which was discovered as part of the Palomar Transient Factory. The SN was located in a dwarf galaxy of magnitude $r = 21.1$ at a redshift $z = 0.0907$. We find that the R -band light curve is a poor proxy for bolometric data and use photometric and spectroscopic data to construct and constrain the bolometric light curve. The derived bolometric magnitude at maximum light is $M_{\text{bol}} = -18.51 \pm 0.2$ mag, comparable to that of SN 1998bw ($M_{\text{bol}} = -18.7$ mag) which was associated with a gamma-ray burst (GRB). PTF10qts is one of the most luminous SNe Ic-BL observed without an accompanying GRB. We estimate the physical parameters of the explosion using data from our programme of follow-up observations, finding that it produced a larger mass of radioactive nickel compared to other SNe Ic-BL with similar inferred ejecta masses and kinetic energies. The progenitor of the event was likely an $\sim 20 M_{\odot}$ star.

Key words: supernovae: general – supernovae: individual: PTF10qts.

*E-mail: emma.walker@yale.edu

† Hubble Fellow.

‡ NSF Astronomy and Astrophysics Postdoctoral Fellow.

1 INTRODUCTION

Type Ic supernovae (SNe Ic) are classified from their optical spectra as having no hydrogen or helium present (for a review of SN classification, see Filippenko 1997). They constitute ~ 10 per cent of the total number of SNe in the local Universe (Li et al. 2011). SNe Ic are believed to be core-collapse events from either a massive Wolf–Rayet star that has lost its outer layers via a wind-loss mechanism (Gaskell et al. 1986) or a less massive star where the envelope has been stripped by a binary companion (Podsiadlowski, Joss & Hsu 1992; Nomoto, Iwamoto & Suzuki 1995). For a recent review of the progenitors of all core-collapse SNe, see Smartt (2009).

One subgroup of SNe Ic, referred to as broad-lined Type Ic supernovae (SNe Ic-BL) or sometimes ‘hypernovae’, exhibits very high line velocities in the spectra, indicating an explosion with high kinetic energy per unit mass. These objects have been linked to gamma-ray bursts (GRBs), initially with the observation that the broad-lined, energetic SN 1998bw was coincident with the long-duration GRB 980425 (Galama et al. 1998). Subsequently, five other spectroscopically confirmed SNe have been identified with GRBs or X-ray flashes (XRFs) between redshifts z of 0.03 and 0.2: GRN 030329/SN 2003dh (Hjorth et al. 2003; Matheson et al. 2003; Stanek et al. 2003), GRB 031203/SN 2003lw (Cobb et al. 2004; Gal-Yam et al. 2004; Malesani et al. 2004; Thomsen et al. 2004), XRF 060218/SN 2006aj (Cobb et al. 2006; Ferrero et al. 2006; Mirabal et al. 2006; Modjaz et al. 2006; Pian et al. 2006; Sollerman et al. 2006), XRF 100316D/SN 2010bh (Chornock et al. 2010; Cano et al. 2011b; Starling et al. 2011; Bufano et al. 2012), and GRB 130702A/SN 2013dx (Cenko et al. 2013; D’Elia et al. 2013; Schulze et al. 2013; Singer et al. 2013). There are also a large and growing number of cases where the optical afterglow of GRBs or XRFs exhibits features typical of (or consistent with) those of SNe Ic-BL (for example, Soderberg et al. 2005; Bersier et al. 2006; Berger et al. 2011; Cano et al. 2011a; Sparre et al. 2011; Melandri et al. 2012; Jin et al. 2013; Levan et al. 2013; Xu et al. 2013).

However, there are also many examples of high-energy SNe Ic for which no associated GRB has been found, including SN 1997ef (Mazzali, Iwamoto & Nomoto 2000) and SN 2002ap (Gal-Yam, Ofek & Shemmer 2002; Mazzali et al. 2002; Foley et al. 2003). It has been suggested that all high-energy SNe Ic form GRBs and that we do not observe the gamma-ray jet because of our viewing angle (Podsiadlowski et al. 2004). This hypothesis is supported by the rates and measurements of the energetics (Smartt et al. 2009), but not by radio observations (Soderberg et al. 2006).

The Palomar Transient Factory (PTF; Law et al. 2009; Rau et al. 2009) was an optical survey of the variable sky using a 7.3 square degree camera installed on the 48 inch Samuel Oschin telescope at Palomar Observatory. PTF conducted real-time analysis and had a number of follow-up programmes designed to obtain colours and light curves of detected transients from a variety of facilities (Gal-Yam et al. 2011). A major science goal of PTF was to conduct an SN survey free from host-galaxy bias and sensitive to events in low-luminosity hosts. Such a survey was particularly suitable to search for SNe Ic-BL, which appear to be more abundant in low-luminosity dwarf galaxies (Arcavi et al. 2010).

In this paper, we present optical photometry and spectra of PTF10qts, an SN Ic-BL. Section 2 describes the observations, which are analysed in Section 3. We summarize our results in Section 4. Throughout the paper, we assume $\Omega_M = 0.3$, $\Omega_\Lambda = 0.7$, and $H_0 = 70 \text{ km s}^{-1} \text{ Mpc}^{-1}$.

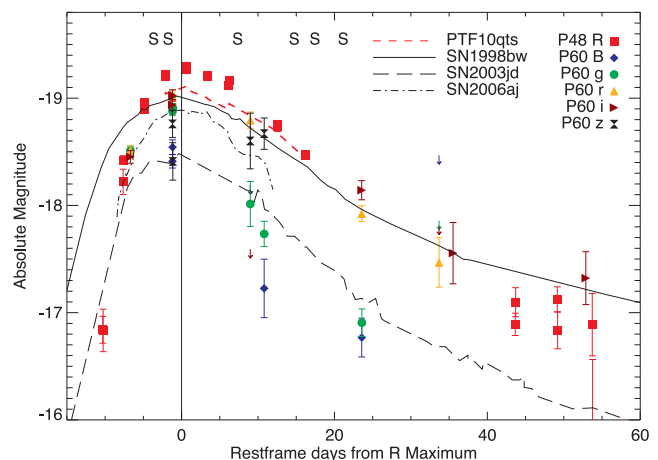


Figure 1. Light curve of PTF10qts from photometry taken on the P48 and P60 telescopes. The data points are given in Table 1 and converted to absolute magnitudes. The solid line represents the R -band light curve of SN 1998bw (Galama et al. 1999), the first GRB-SN, and the dot-dashed line shows the R -band light curve of SN 2006aj (Ferrero et al. 2006), which was accompanied by an XRF. The dashed line shows SN 2003jd (Valenti et al. 2007). No K -corrections have been applied to the individual PTF10qts data, except the long-dashed red line which shows the PTF10qts R_{PTF} points K -corrected using spectra where possible.

2 OBSERVATIONS

2.1 Optical photometry

On 2010 August 05.230 (UT dates are used throughout this paper), PTF10qts was discovered by the Palomar 48 inch telescope (P48; Rahmer et al. 2008) at $R_{\text{PTF}} \approx 20.3 \text{ mag}$;¹ its coordinates were $\alpha(\text{J2000}) = 16^{\text{h}} 41^{\text{m}} 37^{\text{s}}.60$, $\delta(\text{J2000}) = +28^{\circ} 58' 21''.1$. It was also detected again in an image taken later that night on 2010 August 05.305. It was not detected in an image taken three nights previously with a limit of $R_{\text{PTF}} = 20.1 \text{ mag}$. A small, faint ($r = 21.1 \text{ mag}$) host galaxy, object J164137.53+285820.3, is visible in the Sloan Digital Sky Survey (SDSS) catalogue 1.2 arcsec away from the SN. Its redshift, $z = 0.0907$, was measured from $\text{H}\alpha$ and $[\text{O II}]$ narrow emission lines in spectra of PTF10qts. At the host’s distance (414.9 Mpc), the SN offset from the centre of this corresponds to a projected physical distance of 2.4 kpc. No host is discernible in the P48 images. PTF10qts was also observed at the Palomar 60 inch telescope (P60; Cenko et al. 2006) in B , g , r , i , and z , although the cadence for these observations was less than that at the P48.

For observations with the P48, measurements were performed by standard image subtraction, using a deep, good-seeing reference constructed from images taken before the SN exploded. The reference was matched astrometrically to field stars in each image containing the SN and subtracted, and point spread function photometry was then performed. For the P60 data, we employed direct aperture photometry without host-galaxy subtraction, as the host is very faint. The data are calibrated to SDSS magnitudes. A light curve is plotted in Fig. 1 and listed in Table 1. We give the phase in the rest frame relative to R -band maximum determined from fitting the points around maximum light with a parabola. The MJD of the R -band maximum is 55424.6 ± 0.5 (2010 August 16.6). With

¹ $\lambda_c = 6540 \text{ \AA}$.

Table 1. R_{PTF} photometry taken with the P48 and *Bgriz* with the P60. Dates and phases are given in the rest frame relative to R -band maximum, and the photometry has been corrected for Galactic extinction ($E(B - V) = 0.029$ mag). These data are plotted in Fig. 1 after conversion to absolute magnitudes assuming a distance modulus of $\mu = 38.1$ (415 Mpc). The first line of the table is the upper limit of the last non-detection before the SN was discovered.

MJD	Band	Phase (d)	Magnitude	Error
55410.288	R_{PTF}	-13.03	>20.1	
55413.260	R_{PTF}	-10.31	21.25	0.13
55413.304	R_{PTF}	-10.26	21.26	0.20
55416.160	R_{PTF}	-7.65	19.87	0.12
55416.204	R_{PTF}	-7.61	19.67	0.04
55419.175	R_{PTF}	-4.88	19.13	0.03
55419.218	R_{PTF}	-4.84	19.19	0.02
55422.170	R_{PTF}	-2.14	18.87	0.03
55422.214	R_{PTF}	-2.10	18.89	0.02
55425.200	R_{PTF}	0.64	18.79	0.03
55425.242	R_{PTF}	0.68	18.82	0.02
55428.199	R_{PTF}	3.39	18.87	0.02
55428.252	R_{PTF}	3.44	18.88	0.02
55431.236	R_{PTF}	6.18	18.98	0.02
55431.280	R_{PTF}	6.22	18.92	0.03
55438.160	R_{PTF}	12.52	19.34	0.04
55438.204	R_{PTF}	12.56	19.36	0.05
55442.192	R_{PTF}	16.22	19.62	0.03
55442.240	R_{PTF}	16.26	19.62	0.03
55472.110	R_{PTF}	43.65	21.20	0.10
55472.162	R_{PTF}	43.70	20.99	0.14
55478.111	R_{PTF}	49.15	20.97	0.12
55478.154	R_{PTF}	49.19	21.26	0.17
55483.097	R_{PTF}	53.72	21.20	0.29
55483.141	R_{PTF}	53.76	22.19	0.66
55423.197	B	-1.19	19.68	0.06
55423.211	B	-1.18	19.51	0.07
55436.286	B	10.81	20.79	0.27
55450.204	B	23.57	21.25	0.18
55417.201	g	-6.69	19.59	0.04
55423.206	g	-1.19	19.15	0.04
55423.259	g	-1.14	19.20	0.04
55434.307	g	8.99	20.02	0.21
55436.289	g	10.81	20.37	0.12
5450.220	g	23.58	21.12	0.13
55506.082	g	74.80	21.65	0.15
55515.090	g	83.06	21.60	0.35
55423.195	r	-1.20	19.05	0.04
55423.210	r	-1.18	19.03	0.04
55434.302	r	8.99	19.34	0.08
55450.203	r	23.57	20.13	0.07
55461.229	r	33.67	20.66	0.23
55513.092	r	81.22	21.38	0.23
55515.086	r	83.05	21.06	0.19
55417.198	i	-6.69	19.70	0.06
55423.193	i	-1.20	19.14	0.05
55423.208	i	-1.18	19.12	0.05
55450.201	i	23.56	19.93	0.09
55463.233	i	35.51	20.59	0.29
55482.180	i	52.88	20.75	0.25
55506.076	i	74.79	21.42	0.31
55513.090	i	81.22	21.00	0.24
55515.085	i	83.05	21.42	0.35
55423.205	z	-1.19	19.33	0.13
55423.251	z	-1.15	19.75	0.17
55434.305	z	8.99	19.49	0.26
55436.287	z	10.81	19.42	0.15

the non-detection on 2010 August 2 (MJD = 55410.244), we can determine the date of explosion to within 3 d; thus, we constrain the rise time in the R band to 12.7 ± 1.5 d in the observed frame or 11.6 ± 1.4 d in the rest frame.

The data points in Fig. 1 have been corrected for Milky Way extinction, $E(B - V) = 0.029$ mag, using the dust maps of Schlegel, Finkbeiner & Davis (1998) and the extinction curve of Cardelli, Clayton & Mathis (1989). The equivalent width of the Na iD line at zero redshift measured in the spectrum of PTF10qts taken at +7 d is 0.15 ± 0.12 Å, which can be converted to a measurement of extinction via the relation of Turatto, Benetti & Cappellaro (2003). The measured value of $E(B - V) = 0.024 \pm 0.019$ mag is consistent with that determined from the dust maps (but see Poznanski et al. 2011). This is also consistent with the value derived from Poznanski, Prochaska & Bloom (2012) of $E(B - V) = 0.021^{+0.09}_{-0.014}$ mag. We observe no Na iD at the redshift of the SN, so no correction has been applied for host-galaxy extinction. The correction for Milky Way extinction has been applied to the individual points shown in Fig. 1, with no K -corrections (see below).

Fig. 1 also shows the R -band light curves of three other SNe Ic for comparison. SN 1998bw is a broad-lined SN Ic and the first GRB-SN; the values of M_R are similar for both objects. We also include SN 2006aj, which was accompanied by an XRF, and SN 2003jd, which appears to be spectroscopically similar to PTF10qts (see Section 2.2). From the raw R -band light curve, it appears that the SN reaches a more luminous absolute magnitude than SN 1998bw, but with a light-curve width more similar to those of SN 2003jd and SN 2006aj. The long-dashed line shows the R -band light curve of PTF10qts with K -corrections based on the photospheric spectra. This confirms that the R -band light curve is slightly more luminous than that of SN 1998bw, but the decline rate is faster. K -corrections are discussed in more detail in Section 3.2.

2.2 Optical spectroscopy

Follow-up spectroscopy of PTF10qts was carried out at a number of international observatories and is summarized in Table 2. The SN was classified as an SN Ic-BL based on its broad features and lack of obvious hydrogen and helium, and weak silicon in the spectra. The photospheric spectra are plotted in Fig. 2, where all phases are given relative to R -band maximum for each object. Standard IRAF routines as well as custom IDL procedures were used to remove bias and flat-field correct the spectra, as well as to create wavelength and flux solutions for the data. These were then applied to the frames and calibrated spectra were extracted from the data. All spectra of PTF10qts are publicly available via WISEREP² (Yaron & Gal-Yam 2012).

We compare the spectra of PTF10qts to those of other known SNe Ic and SNe Ic-BL in Figs 3–6. Again, all phases are given relative to the R -band maximum for that particular object. We divide our spectra into four periods of observation – pre-maximum, +7 d after R -band maximum, +14 d, and +21 d – consider each of these separately.

Before maximum light, the spectrum of PTF10qts is dominated by broad, high-velocity absorption lines which are blended together. The absorptions at 4400 and 4800 Å are dominated by Fe II. Si II may be seen in the -2 d spectrum and later as the elbow at 5800 Å, but it is blended with other features, making isolation of this feature and a measurement of the photospheric velocity difficult. We also note that

² <http://www.weizmann.ac.il/astrophysics/wiserep/>

Table 2. A summary of spectroscopic observations of PTF10qts. The phase is relative to *R*-band maximum (2010 August 16.6) and then converted to the rest frame. Note that for the Lick/Kast spectrum, the blue side resolution is 4.1 Å (full width at half-maximum, FWHM) and the red side resolution is 9.1 Å (FWHM). The velocities, as plotted in Fig. 7, are determined from the Si II 6355 Å line.

Date (UT)	Phase (d)	Telescope	Range (Å)	Resolution (Å pixel ⁻¹)	Velocity (1000 km s ⁻¹)
2010-08-13	-3.6	P200/DBSP	3505–10 100	5	–
2010-08-15	-1.8	Lick/Kast	3480–10 000	4.1/9.1	19.1 ± 0.75
2010-08-25	+7.4	TNG/DOLORES	3360–8050	2.25	14.4 ± 0.5
2010-09-02	+14.8	P200/DBSP	3440–9850	2	12.0 ± 0.5
2010-09-05	+17.4	P200/DBSP	3440–9850	2	8.5 ± 0.75
2010-09-09	+21.2	KPNO/RC Spec	3620–8140	5.5	–
2011-04-27	+231.7	Keck/LRIS	3100–10 200	2	–

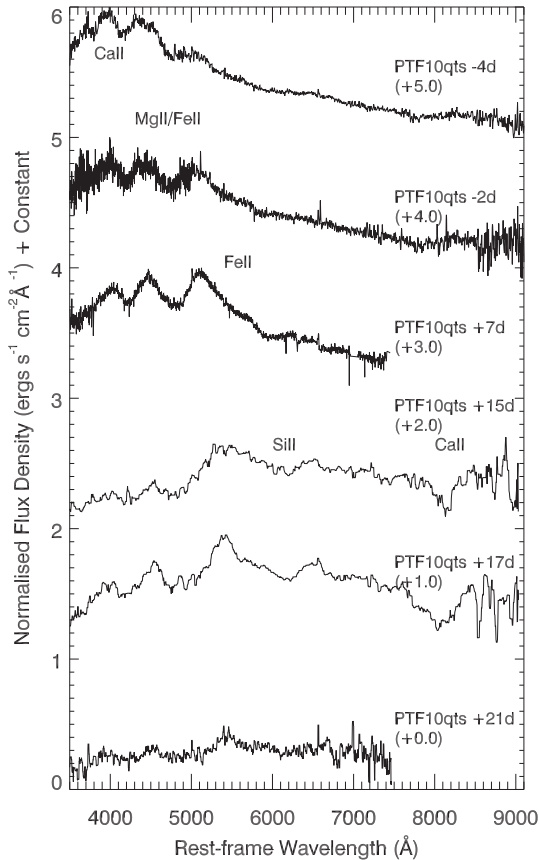


Figure 2. Photospheric spectra of PTF10qts. The phases are given in the rest frame relative to *R*-band maximum. The spectra are labelled showing important species discussed in the text. The number in parentheses shows the offset applied to each spectrum.

visually, the features at 4000–6000 Å of SN 2006aj (Pian et al. 2006) are similar to the early phases of PTF10qts: the spectrum is blue and contains broad absorptions around 4000 Å. We do not see the absorption due to O I in the 7000–7600 Å region visible in spectra of SN 1998bw (Patat et al. 2001) or SN 2004aw (Taubenberger et al. 2006), another SN Ic-BL. The $t = -2$ d spectrum is redder than the $t = -4$ d spectrum, reflecting the fact that the temperature is decreasing as the ejecta expand.

Around a week past maximum brightness, the spectrum of PTF10qts resembles that of SN 2003jd (Valenti et al. 2007), both in the three broad absorption features in the blue and the shape of the continuum in the red.

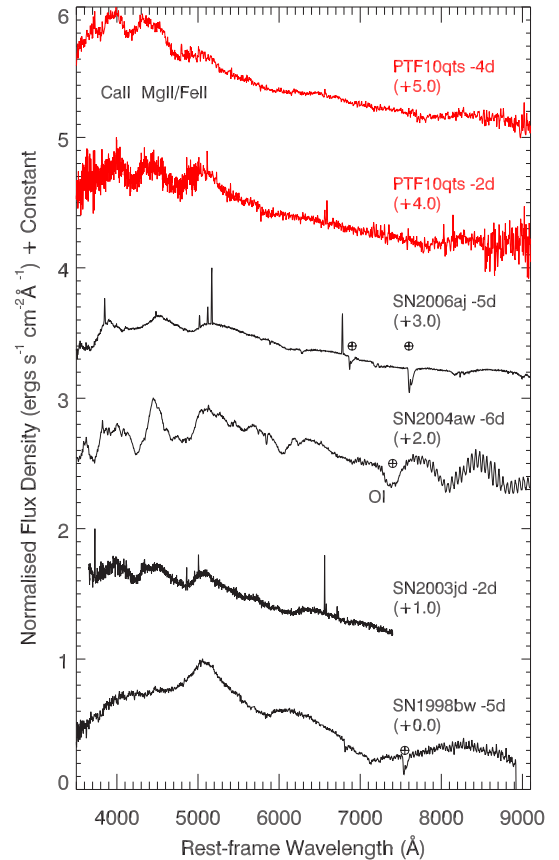


Figure 3. A comparison of spectra before maximum light. Telluric features are marked. The spectra are labelled showing important species discussed in the text. The number in parentheses shows the offset applied to each spectrum.

Our next phase of spectroscopy is around two weeks past maximum light. As seen in Fig. 5, the SN ejecta have expanded sufficiently that we can now see individual features, such as the Si II lines around 6200 Å and strong Ca II absorption at 8100 Å. The velocity of the Ca II near-infrared (NIR) triplet is $\sim 18\,000$ km s⁻¹ (measured from the blueshift of the feature's minimum), which is higher than that for both SN 2003jd and SN 2004aw as shown in the figure. In the blue we also see absorption caused by Mg II, Ca II, and Fe II. Visually the spectra retain their similarity to those of SN 2003jd, SN 2004aw, and to a lesser degree SN 1998bw without O I which is still absent. This may be indicative of a smaller ejecta mass.

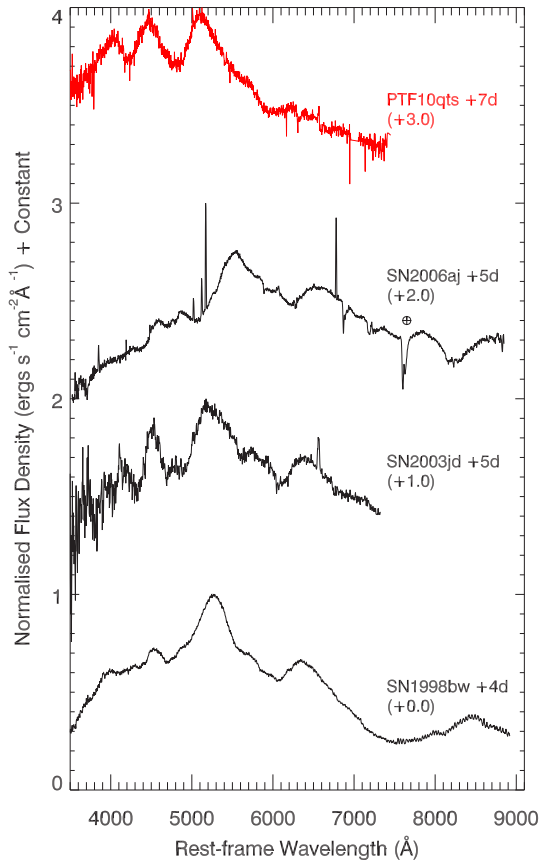


Figure 4. A comparison of spectra around +7 d after maximum light. Telluric features are marked. The number in parentheses shows the offset applied to each spectrum.

The final spectrum of PTF10qts taken during the photospheric phase is shown in Fig. 6. It is quite noisy, but visually the spectral evolution continues to be similar to those of SN 2003jd and SN 2004aw. There may be slight absorption from O I visible in these later spectra. This raises the possibility of a sequence of oxygen masses in SNe Ic-BL ranging from strong in SNe such as SN2004aw, through objects like SN2003jd and finally objects like PTF10qts which show no oxygen.

From this spectral comparison, we conclude that PTF10qts is not a good match to any single well-observed SN Ic-BL over its entire evolution, although at some phases there appear to be reasonable matches to other known SNe Ic-BL. PTF10qts lacks the very high velocities (i.e. energy per unit mass) of SN 1998bw, and the spectral features (related to element abundances) do not match those seen in the lower velocity examples of SN 2003jd, SN 2004aw, and SN 2006aj.

3 DISCUSSION

3.1 Velocity determination

Before determining the physical parameters of this SN, it is necessary to constrain the SN photospheric velocity at maximum light, which is typically characterized by the minimum of the blueshifted absorption of the Si II feature around ~ 6150 Å. However, as seen below, we use two different methods which involve two different dates for maximum light and we do not have the spectral coverage around these times to measure values directly from spectra, along with the

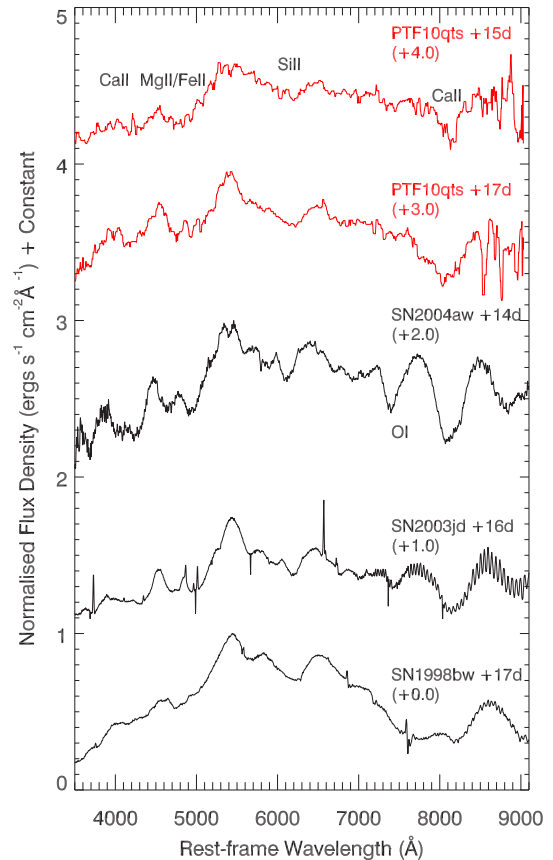


Figure 5. A comparison of spectra around +14 d after maximum light. The spectra are labelled showing important species discussed in the text. The number in parentheses shows the offset applied to each spectrum.

additional problem of the SN features being blended together so the Si II line which is thought to give a clear determination of the photospheric velocity is not always visible as a separate feature.

In Fig. 7, we show the velocities of PTF10qts (bowtie) compared to a number of other types of SNe, including the two we will use for analogues – SN1998bw and SN2006aj. We can define the velocity to use in later analysis in different ways such as the velocity at maximum light in the *R* band or the velocity at the maximum of the bolometric light curve. The time between explosion and maximum varies between SNe, but if we wanted a uniform time, we could also take a fixed date after explosion.

Applying these three methods to PTF10qts reveals that both the *R*-band and bolometric maxima fall between the first two velocity measurements from the spectra. We interpolate linearly between the velocities measured at -1.8 d and $+7.4$ d as given in Table 2 and assign PTF10qts a photospheric velocity of $17\,000 \pm 1500$ km s $^{-1}$. Due to the small difference in rise times for the bolometric and *R*-band light curves for SN1998bw and SN2006aj, we use two different velocities for these objects in the following sections and assign an error of ± 1000 km s $^{-1}$ to each one. We have been conservative with the velocity errors, but they are only a small contribution to the final error on the physical parameters we derive below.

3.2 *R* band as a proxy for bolometric

We first attempt to use the *R*-band light curve, which has the best phase coverage, to estimate some of the physical parameters of the SN explosion. It has also been suggested that the *R* band can be used

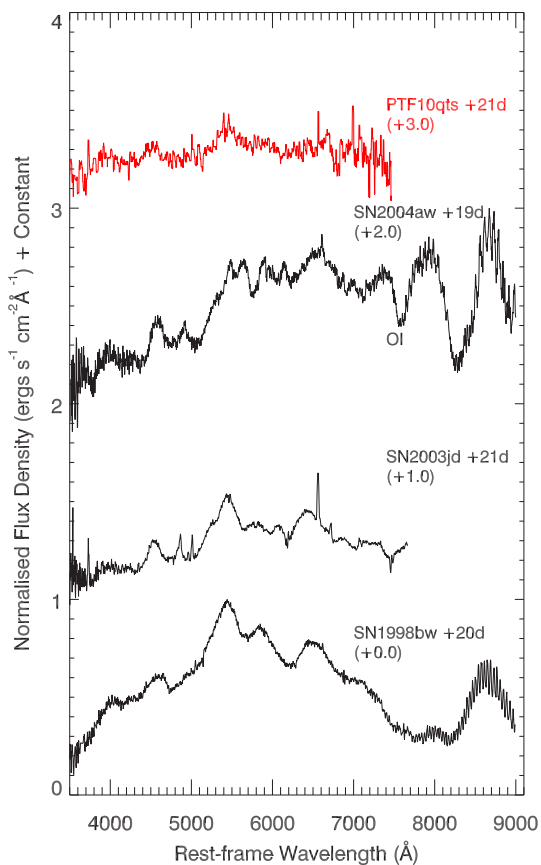


Figure 6. A comparison of spectra around +21 d after maximum light. The spectra are labelled showing important species discussed in the text. The number in parentheses shows the offset applied to each spectrum.

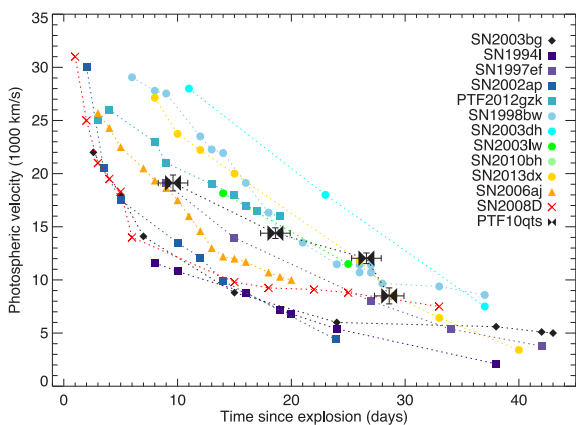


Figure 7. A plot of the photospheric velocities of SNe at different times after explosion. Different symbol shapes correspond to different types of SNe: diamond – I Ib; square – Ic/Ic-BL; circle – GRB/SNe; triangle – XRF/SN Ic; cross – XRF/SN Ib; and bowtie – PTF10qts. This figure is augmented from the one produced in Mazzali et al. (2008).

as a proxy for bolometric when calculating the physical parameters of the explosion (Drout et al. 2011). We employ a well-studied example as an analogue and scale the physical parameters based on the modelling of that object. Ideally, the analogue would match the light curve and the spectrum. This is particularly important for SNe

Ic-BL, as the kinetic energy is dominated by the broadest parts of the lines. These features are usually blended; thus, as well as matching the velocities, it is important to match the spectra to reduce the error when scaling the parameters.

Unfortunately, as discussed above, there is no single good analogue of PTF10qts. Instead, we take two examples for which bolometric light curves and other physical parameters are well modelled, and we use their properties to estimate the ejecta mass M_{ej} , kinetic energy E_K , and nickel mass $M(^{56}\text{Ni})$ of PTF10qts. We adopt SN 1998bw, as this is the most similar in absolute R magnitude to PTF10qts at maximum light ($R = -19.16$ mag for SN 1998bw compared to $R_{\text{PTF}} = -19.30$ mag for PTF10qts), and also SN 2006aj, which is similar spectroscopically. Radiative transfer models of their light curves have been developed to derive the physical parameters of these explosions (Nakamura et al. 2001; Mazzali et al. 2006a).

In order to compare properly PTF10qts with existing samples in the literature, we use photometry and spectra to measure $R - I$ colours and obtain the transformation from magnitudes in R_{PTF} to R as in Ofek et al. (2012) and Jordi, Grebel & Ammon (2006). We find that given the sparse light-curve coverage, it is not possible to infer a relationship between $R - I$ and phase. We therefore assume a constant value of $R - I = 0.24 \pm 0.12$ mag, which is the mean of all the measured values. This corresponds to $R = R_{\text{PTF}} - 0.14 \pm 0.01$ mag, where the quoted uncertainty comes only from the colour term.

Given the redshift of PTF10qts, the observed R band is very different from the observed R band of the local comparison of SNe we have used. To compensate for this, we calculate K -corrections using the spectra of PTF10qts following Humason, Mayall & Sandage (1956). The spectra acquired on August 25 (TNG) and September 9 (KPNO) fall short of covering the full R band by a few hundred angstroms when shifted to the rest frame. Therefore, at wavelengths longer than their red end, we assumed that their behaviour is similar to the spectra taken on August 15 (Lick) and September 2 (P200), respectively, based on the similarity of the spectra at bluer wavelengths. We then interpolated the measurements to obtain K -corrections at 0 and +15 d relative to R -band maximum. The calculated values are -0.174 and -0.027 , respectively.

We interpolated the R -band light curve of PTF10qts to obtain final values of $R(0) = -19.27 \pm 0.06$ and $R(15) = -18.69 \pm 0.06$ mag. The uncertainties include measurement errors, uncertainties in the K -correction, and conversion from R_{PTF} to R . We therefore find $\Delta m_{15}(R) = 0.58 \pm 0.08$ mag for PTF10qts. This is similar to that of SN 1998bw ($\Delta m_{15}(R) = 0.56$ mag), but much smaller than that of SN 2006aj ($\Delta m_{15}(R) = 0.86$ mag). Note that the K -corrected values in R differ from the light curve for PTF10qts shown in Fig. 1, as that is for R_{PTF} .

Using Arnett (1982), we know the following relations for an SN at maximum light:

$$M_{\text{ej}} \propto \tau^2 v_{\text{phot}}, \text{ and} \quad (1)$$

$$E_K \propto \tau^2 v_{\text{phot}}^3, \quad (2)$$

where τ is the light-curve width which is proportional to $1/\Delta m_{15}(R)$ and v_{phot} is the photospheric velocity. We have chosen to use $\Delta m_{15}(R)$ instead of τ for this measurement because of the uncertainty in the K -corrections before the first epoch of spectroscopy. For v_{phot} , we adopt the values of $15\,500$ km s $^{-1}$ for SN 2006aj and $18\,000$ km s $^{-1}$ for SN 1998bw. As discussed above, we have assumed $v_{\text{phot}} = 17\,000$ km s $^{-1}$. With equations (1) and (2), we can calculate the physical parameters for PTF10qts assuming that

Table 3. A summary of the physical parameters assumed for SN 1998bw and SN 2006aj, and those derived for PTF10qts first in the *R* band and then using the bolometric light curve. E_K is the kinetic energy and L_i is the peak luminosity in either *R* or bolometric. The parameters for SN 1998bw and SN 2006aj are either measured from their published light curves or, in the case of E_K , v , M_{ej} , and $M(^{56}\text{Ni})$, taken from the modelling in Nakamura et al. (2001) and Mazzali et al. (2006a), respectively.

Parameter	SN 1998bw	SN 2006aj	PTF10qts SN 1998bw-like	PTF10qts SN 2006aj-like
<i>R</i> band				
$\Delta m_{15}(R)$ (mag)	0.56	0.86	0.58 ± 0.18	0.58 ± 0.18
v (km s ⁻¹)	$19\,000 \pm 1000$	$15\,000 \pm 1000$	$17\,000 \pm 1500$	
L_R (erg s ⁻¹)	1.87×10^{42}	1.08×10^{42}	$(2.10 \pm 0.05) \times 10^{42}$	
t_R (d)	17	10.5	11.6 ± 1.3	
M_{ej} (M_\odot)	10 ± 1	1.8 ± 0.8	8.3 ± 2.6	4.3 ± 1.3
E_K (erg)	$(50 \pm 10) \times 10^{51}$	$(2 \pm 1) \times 10^{51}$	$(33.4 \pm 14.4) \times 10^{51}$	$(6.1 \pm 3.9) \times 10^{51}$
$M(^{56}\text{Ni})$ (M_\odot)	0.43 ± 0.05	0.2 ± 0.04	0.34 ± 0.09	0.42 ± 0.08
Bolometric				
τ (d)	21.7 ± 0.5	16.6 ± 0.5	16.8 ± 1	
v (km s ⁻¹)	$20\,000 \pm 1000$	$16\,000 \pm 1000$	$17\,000 \pm 1500$	
L_{bol} (erg s ⁻¹)	8.32×10^{42}	5.58×10^{42}	$(7.7 \pm 1.4) \times 10^{42}$	
t_{bol} (d)	15	9.6	13.4 ± 2.3	
M_{ej} (M_\odot)	10 ± 1	1.8 ± 0.8	5.1 ± 0.9	2.0 ± 0.3
E_K (erg)	$(50 \pm 10) \times 10^{51}$	$(2 \pm 1) \times 10^{51}$	$(18.5 \pm 6.6) \times 10^{51}$	$(2.5 \pm 1.4) \times 10^{51}$
$M(^{56}\text{Ni})$ (M_\odot)	0.43 ± 0.05	0.2 ± 0.04	0.36 ± 0.1	0.36 ± 0.08

it is analogous to either SN 1998bw or SN 2006aj.³ The resulting parameters are given in Table 3.

We propagate errors in $\Delta m_{15}(R)$, the values of the analogue M_{ej} and E_K , and on measuring the velocities through the equations to obtain an uncertainty for each parameter estimate. We note that the largest contribution to the error budget comes from the errors in the quantities of the analogues, not from anything measured from the PTF10qts light curve. There is a large discrepancy between the values of both quantities when using the two different analogues.

The amount of nickel produced can be estimated from the peak bolometric luminosity following the assumptions of Arnett (1982). Assuming a constant bolometric correction from the *R* band as in Drout et al. (2011), we can instead use the *K*-corrected magnitude in *R*. All three SNe have different rise times, so we introduce a correction to account for the varying number of *e*-folding times for primarily ⁵⁶Ni, which has a half-life of 6.08 d, and also for the decay product ⁵⁶Co ($t_{1/2} = 77.23$ d), assuming that there is no ⁵⁶Co produced in the SN explosion itself. For an *R*-band luminosity L_R and a nickel mass $M(^{56}\text{Ni})$, we find the relation

$$L_R \propto M(^{56}\text{Ni}) \left(\frac{E_{\text{Ni}}}{\tau_{\text{Ni}}} e^{-\frac{t_R}{\tau_{\text{Ni}}}} + \frac{E_{\text{Co}}}{\tau_{\text{Co}}} \frac{\tau_{\text{Co}}}{\tau_{\text{Co}} - \tau_{\text{Ni}}} \left[e^{-\frac{t_R}{\tau_{\text{Co}}}} - e^{-\frac{t_R}{\tau_{\text{Ni}}}} \right] \right), \quad (3)$$

where t_R is the rise time in the *R* band, and τ_{Ni} and τ_{Co} are the respective mean lifetimes for ⁵⁶Ni and ⁵⁶Co, where $\tau_i = t_{1/2}/\ln 2$. E_{Ni} and E_{Co} are the energies released by a unit mass of Ni and Co, respectively. The energy per decay is 1.7 MeV for ⁵⁶Ni and 3.67 MeV for ⁵⁶Co. As for the parameters estimated in Section 3.2, we use the values measured for SN 1998bw and SN 2006aj to provide two estimates of the nickel mass which we can then combine. The individual values for each SN are given in Table 3.

³ Note that for SN 2006aj, the light-curve data for the *R* band end at +12 d relative to *R*-band maximum, but the bolometric light curve extends to +14 d owing to the availability of data in other filters. We evaluated bolometric magnitudes from these by assuming a constant bolometric correction with respect to the *V* band. We obtain the same result if we extrapolate just the *R*-band light curve over the longer interval.

This estimate is significantly different from the value obtained using the relationship in Drout et al. (2011, $\sim 0.2 M_\odot$), despite the fact that PTF10qts is not unusual in either its $\Delta m_{15}(R)$ or M_R values (see their fig. 22). This is because their relation relies purely on the absolute magnitude of the SN at maximum and does not take into account differences in rise times. In this study, we see that PTF10qts has a similar peak magnitude in the *R* band to SN1998bw, but the rise time is ≈ 5.5 d shorter. This would imply a much reduced nickel production in PTF10qts which is not reflected in the Drout et al. (2011) estimation.

The fact that we obtain an even lower value with the Drout et al. (2011) formula is curious; however, it also predicts a lower nickel mass for SN1998bw at $0.34 M_\odot$. The value for SN2006aj is in good agreement with that obtained from the modelling – $0.19 M_\odot$. We attribute this to the fact that SN1998bw has a much longer rise time than all of the SNe used in Drout et al. (2011), whereas SN2006aj has a more typical rise time.

The simplification of assuming $L \propto M(^{56}\text{Ni})/\tau$ is not appropriate for comparing SNe with significantly different rise times or where the SNe deviate from parabolic light curves where $\tau \propto 1/\Delta m_{15}(R)$. We can see that this is not the case for both *R*-band and bolometric light curves in Figs 1 and 8.

These results clearly show that it is not possible to use just the *R* band to determine the physical parameters of this SN and so we would caution the extension of the Drout et al. (2011) relations to other SNe, in particular where the rise time is poorly constrained or differing from ≈ 10 – 12 d. Instead we now focus on the generation of a bolometric light curve.

3.3 Bolometric light curve

We combine photometric and spectroscopic data to construct a pseudo-bolometric⁴ light curve, as this will remove the assumption

⁴ We use the term pseudo-bolometric as the light curve we generate is from the UV to NIR only and cannot be described as truly bolometric as it excludes contributions at wavelengths outside this region, particularly gamma-rays.

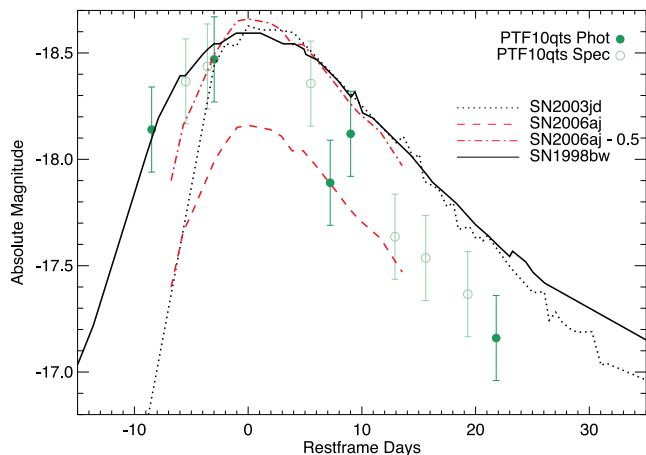


Figure 8. The bolometric light curve of PTF10qts calculated from spectroscopic points or from photometry. Also shown for comparison are light curves of SN 1998bw, SN 2006aj, SN 2006aj -0.5 mag, and SN 2003jd.

that the bolometric corrections from the R band for PTF10qts and either analogue are the same at all phases.

Bolometric fluxes were computed from the six spectra by integrating their dereddened signal in the interval 4000–8500 Å. As when calculating the K -corrections, we extend the August 25 (TNG) and September 9 (KPNO) spectra in the red to cover this range of wavelengths. We have also computed bolometric fluxes from the photometry at all epochs in which at least three bands were covered. After correcting for Milky Way reddening, we converted them to fluxes according to Fukugita et al. (1996), and then splined and integrated them in the observed 4000–8500 Å range. In the rest frame, the red boundary of this integration interval corresponds to ~ 7800 Å; thus, we have increased all bolometric fluxes by 15 per cent to account for the ultraviolet (UV) and NIR contributions (based on comparisons to other SNe that have been observed accurately both in the optical and NIR). Considering the uncertainty related to this assumption and the lack of UV information, we associate an uncertainty of 20 per cent with each bolometric flux.

When combining the data points generated by these two different routes, we noted that the spectroscopically derived points were systematically offset by a small amount to brighter magnitudes than the photometrically derived points. We attribute this offset to inconsistencies in the two methods used to derive the individual points. To align the spectroscopically generated points, we used the bolometric light curve of SN 1998bw (itself generated via the photometric route) and fitted it to just the photometrically derived data points of PTF10qts, allowing a temporal ‘stretch’ and constant-magnitude shift-up and shift-down. Treating this warped light curve as a template, we then used χ^2 minimization to apply a constant shift to the spectroscopically derived data to bring them in line with the photometrically derived points. The final bolometric light curve is reported in Fig. 8, where phases are plotted relative to the date of bolometric maximum, which occurs 1.84 rest-frame days after R -band maximum.

Comparing the shapes of bolometric light curves is another approximate way to examine the physical similarity of PTF10qts to other SNe Ic-BL: supernovae with similar physical properties will have similarly shaped light curves. In Fig. 8, we show PTF10qts with the bolometric light curves of other SNe Ic-BL so that the dates of maximum align. We see that the bolometric light curve of PTF10qts is most similar to that of SN 1998bw, although the later points of PTF10qts may decline slightly faster, implying a lower

nickel mass in PTF10qts. SN 2006aj is also a good match around maximum if it is made brighter by 0.5 mag, although the light curve is narrower, so we would expect a higher kinetic energy and nickel mass in PTF10qts than SN 2006aj. We can use these observations as a sanity check when deriving physical properties from the bolometric light curve. We also show that SN 2003jd, which is a good match at some spectroscopic phases, is a poor match to the bolometric light curve before maximum brightness, again showing that spectroscopic similarity does not always mean the physics of the SN explosion are the same.

We estimate the physical parameters using the relationships discussed in Section 3.2, but now using the bolometric quantities. With bolometric data significantly before maximum brightness, we can switch to using τ , the light-curve width, instead of just the post-maximum $\Delta m_{15} \propto 1/\tau$, which we have shown to be only an approximation. We define τ to be the width at peak magnitude minus 0.5 mag. This should better reflect the differences between the SN light curves because, as Fig. 8 shows, after maximum the slopes of SN 1998bw, SN 2006aj, and PTF10qts are very similar, but before maximum, they differ significantly. For PTF10qts, SN 1998bw, and SN 2006aj, we measure $\tau = (16.8 \pm 1, 21.7 \pm 0.5, 16.6 \pm 0.5)$ d, where now PTF10qts is much less similar to SN 1998bw and more like SN 2006aj.

We measure the quantities when using both the SN 1998bw and SN 2006aj bolometric light curves, and these results are given in Table 3. We again see how important it is to choose an analogue which matches both the spectroscopy and the light curve, as the estimates of the physical parameters based on SN 1998bw and SN 2006aj do not agree. This is due to the different values of E_K/M_{ej} and mass of ^{56}Ni for the two analogues. We take the weighted mean of the two analogues as the best estimate of the physics of PTF10qts: $M_{ej} = 2.3 \pm 0.3 M_\odot$ and $E_K = (3.2 \pm 1.4) \times 10^{51}$ erg. We also derive a nickel mass of $M(^{56}\text{Ni}) = 0.36 \pm 0.07 M_\odot$. The measurements of the ejecta mass and the kinetic energy are lower than those found using just the R band, and the nickel mass is slightly higher. We note that these estimates are similar to those for SN 2010ah (Mazzali et al. 2013), but the spectra are very different.

To estimate the zero-age main sequence (ZAMS) mass of the progenitor, we use the models of Sugimoto & Nomoto (1980) and assume a remnant mass of $2 M_\odot$ as in their models. PTF10qts corresponds to a progenitor star with a ZAMS mass of $\sim 20 \pm 2 M_\odot$.

3.4 Nebular spectrum

We can also estimate the nickel mass from the nebular spectrum, which was obtained with LRIS at the Keck-I telescope 230 rest-frame days after R -band maximum. This is shown in Fig. 9 with a continuum subtracted from it. Also shown is a synthetic spectrum. The observed spectrum has a low signal-to-noise ratio, so the resultant model fit parameters should not be used to draw any firm conclusions. We used a code for the synthesis of nebular spectra as described by Mazzali et al. (2001). The synthetic spectrum was obtained using $M(^{56}\text{Ni}) = 0.35 \pm 0.1 M_\odot$, which is in good agreement with the estimate from the bolometric light curve. The red part of the spectrum also appears to indicate a low oxygen mass ($\sim 0.7 M_\odot$) in the SN, which would support the lack of detection in the post-maximum spectra (Fig. 5); however, the blueshifted profile of the [O I] emission suggests that the line may not yet be optically thin. The oxygen mass may therefore be underestimated, although we tried to take this into account in the model by requiring a stronger line than the observed one.

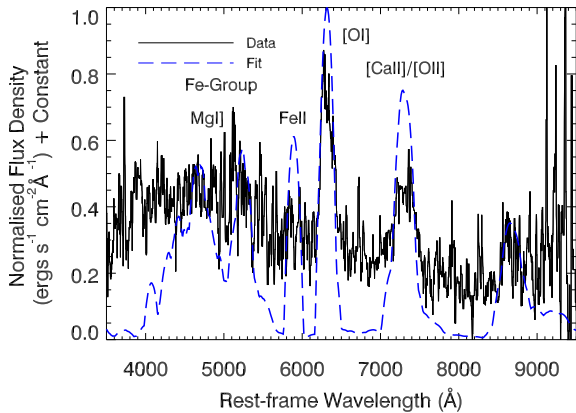


Figure 9. A spectrum of PTF10qts obtained at the Keck 10 m telescope 230 d after *R*-band maximum. A continuum has been subtracted from the data to account for host-galaxy contamination. The dashed line is a fit to the spectrum.

3.5 Comparison to other SNe Ic

Table 4 contains a compilation of all SNe Ic-BL published in the literature for which physical parameters have been derived, as well as a few intermediary cases in the region between normal SNe Ic and SNe Ic-BL. Those SNe with which GRB events have been associated are marked by an asterisk. For SN 2010bh, we have used the models of Sugimoto & Nomoto (1980) to infer the progenitor properties from the published energetics. PTF10qts is unremarkable among this type of SN in terms of the kinetic energy and ejecta mass, but the nickel mass is towards the higher end of the observed range.

To explore this more fully, in Fig. 10 we compare PTF10qts to the trends published by Mazzali et al. (2013) for energetic SNe and hypernovae where all physical parameters and the progenitor mass have been determined. There appears to be a strong relation between the progenitor mass and the kinetic energy of the SN, and PTF10qts lies on this trend. For example, SN 2006aj has the same progenitor mass, and a similar kinetic energy is derived from the bolometric light curve. The relationship between the mass of synthesized ^{56}Ni is much looser, and PTF10qts lies away from the apparent trend, producing more nickel than would be expected for its progenitor mass. In fact, PTF10qts has an ejected nickel mass comparable to those events classified as hypernovae. We thus call PTF10qts a nickel-rich SN Ic-BL.

Although PTF10qts is not spectroscopically similar to SN 1998bw, it is still photometrically similar and the event was clearly energetic. We used Interplanetary Network (IPN) data to search for a possible GRB companion to PTF10qts in case gamma-rays had been detected by any of the orbiting satellites. The IPN includes *Mars Odyssey*, *Konus-Wind*, *RHESSI*, *INTEGRAL* [Spectrometer for INTEGRAL AntiCoincidence Shield (SPI-ACS)], *Swift-Burst Alert Telescope* (BAT), *Suzaku*, *AGILE*, *MESSENGER*, and *Fermi* [Gamma-ray Burst Monitor (GBM)].

The date of the PTF10qts explosion is uncertain; we know only the first detection of the SN, 2010 August 5. The observed rise time of PTF10qts is estimated to be 12.7 ± 1.5 d. We searched for a GRB around 16 days before PTF10qts maximum light (allowing for any delay between a GRB and the emergence of the SN). This corresponds to a date range of 2010 August 1–5.

During this period, six bursts were detected by the nine spacecraft of the IPN. During the same period, there were also 14 unconfirmed bursts which have been excluded from further analysis. The sample

also excludes bursts from known sources such as anomalous X-ray pulsars and soft gamma repeaters.

Of these six bursts, three were observed with the coded fields of view of the *Swift*-BAT or *INTEGRAL* IBIS instruments, which have a positional accuracy of several arcminutes. These bursts were inconsistent with the position of PTF10qts. Two were observed either by the *Fermi* GBM alone or by the *Fermi* GBM and one or more near-Earth spacecraft. The GBM error contours are not circles, although they are characterized as such, and they have at least several degrees of systematic uncertainties associated with them. Since no other confidence contours are specified, it is difficult to judge accurately the probability that any particular GBM burst is associated with the SN. In this analysis, we have simply multiplied the 1σ statistical-only error radius by 3 to obtain a rough idea of the 3σ error contours. One further event was observed by *Konus* and *MESSENGER*, and in this case the probability that this burst was due to PTF10qts is 0.04, excluding this as burst as coincident with the SN.

The total area of the localizations of the six bursts was $\sim 0.04 \times 4\pi$ sr. This implies that there is a very low probability of finding an unassociated gamma-ray source coincident with our SN during the time window we are investigating.

There is another approach to the probability calculation. Since only 0 or 1 GRB in our sample can be physically associated with the SN, we can calculate two other probabilities. The first is the probability that, in our ensemble of six bursts, none is associated by chance with the SN. Let P_i be the fraction of the sky which is occupied by the localization of the i th burst. Then the probability that no GRB is associated with the SN is

$$P(\text{No GRB}) = \prod_i (1 - P_i). \quad (4)$$

For our sample, this probability is 0.96.

The second probability is that any one burst is associated by chance with the SN, and that all the others are not:

$$P(\text{One GRB by chance}) = \sum_i P_i \prod_{i \neq j} (1 - P_j). \quad (5)$$

For our sample, this probability is 0.004.

This analysis covers a very narrow range of dates for any potential GRB burst. If we extend the search period to the 30 d preceding the first optical detection of PTF10qts, there is still no statistically significant detection of any gamma-rays associated with the SN event. In light of this, we assume that we have not detected any gamma-rays associated with PTF10qts.

4 CONCLUSIONS

We have presented optical follow-up data for the SN Ic-BL PTF10qts, discovered at $z = 0.0907$ by the PTF. We find that the *R*-band light curve of PTF10qts is not a good representation of the bolometric light curve; hence, we used photometric and spectroscopic data to produce a pseudo-bolometric light curve from which to estimate the physical parameters of the SN explosion.

PTF10qts appears to be an SN Ic-BL from a progenitor of $\sim 20 M_\odot$, which is a smaller mass than some other SN Ic-BL events, such as SN 1998bw, SN 2003dh, and SN 2003lw for which the progenitors are all believed to be $> 35 M_\odot$. However, PTF10qts produces a similar amount of ^{56}Ni to these events, which are all associated with GRBs. A search of IPN data found no evidence for gamma-rays associated with the SN event though. PTF10qts falls on the general trends of SNe Ic in terms of the relation between

Table 4. Summary of the explosion properties of well-studied SNe Ic-BL.

Object	Host	Distance (Mpc)	Distance method ^a	$M(^{56}\text{Ni})$ (M_{\odot})	E_K (10^{51} erg)	M_{ej} (M_{\odot})	Velocity ^b (km s^{-1})	M_{rem} (M_{\odot})	ZAMS (M_{\odot})	Method ^c	References
SN 1997ef	UGC 04107	48.95	z	0.15	8	10	9500	2.4	30–35	M	1
SN 1998bw*	ESO 184082	35.1	z	0.4	50	10	10 500	>3.0	40	M	2
SN 2002ap	NGC 0628	8	TF	0.07	4–10	2.5–5		2.5	20–25	M	3
SN 2003dh*	anonymous	810.3	z	0.38	37.5	7.5	18 000	2.4	25–40	M	4, 5
SN 2003jd	MCG 0159021	76.7	z	0.36 ± 0.04	7^{+3}_{-2}	3.0 ± 0.5	13 500	>3.0	22–28	M	6
SN 2003lw*	anonymous	487.4	z	0.55 ± 0.1	60 ± 10	13 ± 2	18 000	>3.0	40–50	M	7
SN 2004aw	NGC 3997	72.5	z	0.3 ± 0.05	$3.5 - 9.0$	$3.5 - 8.0$				M	8
SN 2005kz	MCG 0834032	114	z	$0.47^{+0.31}_{-0.19}$	$2.2^{+1.5}_{-0.8}$				F	I (94I)	9
SN 2006aj*	anonymous	146.7	z	0.21	2	1.8	15 000	1.4	20	M	10, 11
SN 2007bg	anonymous	152.1	z	0.12 ± 0.02	4 ± 1	1.5 ± 0.5	9000		F	F	12
SN 2007D	UGC 02653	97	z	1.5 ± 0.5	$1.5^{+0.8}_{-0.5}$				F	F	13
SN 2007ru	UGC 12381	62	z	0.4	5^{+3}_{-3}	$1.3^{+1.1}_{-0.8}$	20 000			I (94I/98bw)	14
SN 2009bb	NGC 3278	46.7	z	0.22 ± 0.06	18 ± 7	4.1 ± 1.9	15 000			F/I (02ap)	15
SN 2009nz*	anonymous	2765.1	z	0.35	2.3	1.4	17 000			D	16, 17
SN 2010ah	SDSS J114402.98+554122.5	221.4	z	0.25 ± 0.05	12 ± 4	3.3 ± 1	18 000	1.5–3	24–28	I (98bw/02ap)	18
SN 2010ay	SDSS J123527.19+270402.7	301.5	z	$0.9^{+0.2}_{-0.1}$	11	4.7	19 200			D	19
SN 2010bh	anonymous	264.9	z	0.12 ± 0.02	9.7 ± 5.5	3.2 ± 1.6	$1.74 \times 2006\text{aj}$			I (06aj)	20
PTF10qts	SDSS J164137.53+285820.3	414.9	z	0.10 ± 0.01	13.9 ± 0.6	2.24 ± 0.08	25 000	1.4	20–23	F	21
SN 2012au	NGC 4790	23.5	TF	0.21 ± 0.03	24 ± 7	2.6 ± 0.23	$25\ 000 - 31\ 000$	2	20 ± 2	F	22
				0.36 ± 0.07	2.7 ± 0.9	2.1 ± 0.2	15 000			I (98bw/06aj)	23
				0.3	10	3–5	15 000			F	

(*): accompanied by a GRB or XRF.

^aTF: Tully–Fisher relation; z: luminosity distance converted from redshift using the same cosmology as this paper.

^bPhotospheric velocity derived from spectra.

^cRefers to the method(s) used for calculating the physics of the explosion. M: radiative transfer modeling, F: fitting of an analytical model as in Ref. 6, I: interpolation using other SNe, D: relations from Ref. 9.

^dDerived quantity equal to $M_{\text{ej}}^{2/3} E_K^{-1/4}$.

References — 1: Iwamoto et al. (2000), 2: Nakamura et al. (2001), 3: Mazzali et al. (2002), 4: Mazzali et al. (2003), 5: Deng et al. (2005), 6: Valenti et al. (2007), 7: Mazzali et al. (2006b), 8: Taubenberger et al. (2006), 9: Drout et al. (2011), 10: Mazzali et al. (2006), 11: Pian et al. (2006), 12: Young et al. (2009), 13: Sahu et al. (2009), 14: Pignata et al. (2011), 15: Berger et al. (2011), 16: Corsi et al. (2011), 17: Mazzali et al. (2013), 18: Sanders et al. (2012), 19: Bufano et al. (2012), 20: Cano et al. (2011b), 21: Olivares et al. (2012), 22: this work, 23: Milisavljevic et al. (2013).

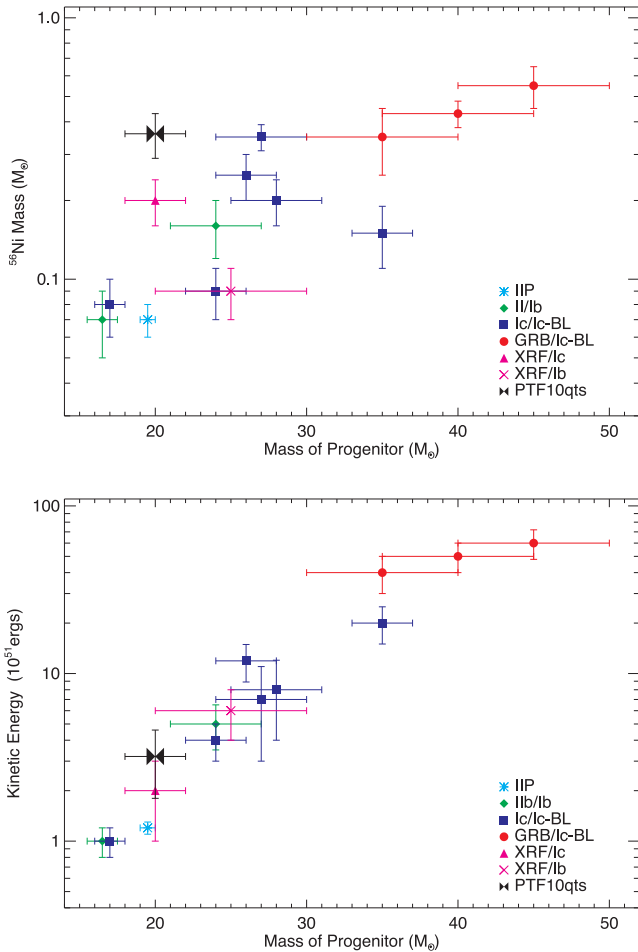


Figure 10. A reproduction of the plots from Mazzali et al. (2013) with the addition of new data. The objects in the plot are (in order of ascending progenitor mass) SN IIP – SN 1987A; SNe IIb/Ib – SN 1993J, SN 2003bg; SNe Ic/Ic-BL – SN 1994I, SN 2002ap, SN 2010ah, SN 2003jd, SN 2004aw, SN 1997ef; GRB/SNe Ic-BL – SN 2003dh, SN 1998bw, SN 2003lw; XRF/SN Ic – SN 2006aj; and XRF/SN Ib – SN 2008D. PTF10qts is shown as the bowtie symbol.

progenitor mass and kinetic energy, but for its ZAMS mass of $\sim 20 M_{\odot}$, it produced more ^{56}Ni than would be expected. This is evidenced by its luminous light curve, but its narrower light-curve width when compared to SN 1998bw ($\tau = 21.7$ d compared to $\tau = 16.8$ d). We note that the ^{56}Ni masses we obtained by analogy with SN 1998bw and SN 2006aj using the *R*-band light curve (line 7 of Table 3) are different from those calculated via the bolometric light curve (line 14 of Table 3). This indicates that the *R*-band light curve is not a completely reliable proxy for the bolometric light curve, and the latter is preferable when evaluating physical parameters.

We would caution the use of physical relationships based on monochromatic light curves for use as anything other than a first approximation. This is because assumptions such as constant opacity, constant bolometric correction, and $L \propto 1/\tau$ are oversimplifications. In this study, we have compared two methods using *R*-band and bolometric data. We find that the bolometric method is more suitable, but is still only an approximation. A constraint on the time of explosion is required for this to provide anything other than a lower limit on the nickel mass. The physical parameters of an SN

explosion of this type can *only* be determined with full modelling of the light curve and spectra.

We encourage future observations of similar objects discovered early and with light curves and spectral coverage across the entire UV–optical–infrared range in order to better understand their nature.

ACKNOWLEDGEMENTS

We acknowledge financial contributions from contract ASI I/016/07/0 (COFIS), ASI I/088/06/0, and PRIN INAF 2009 and 2011. PTF is a collaboration of Caltech, LCOGT, the Weizmann Institute, LBNL, Oxford, Columbia, IPAC, and UC Berkeley. Collaborative work between AG and PAM is supported by a Minerva grant. The Weizmann PTF membership is supported by the ISF via grants to AG. Joint work of AG and SRK is supported by a BSF grant. AG also acknowledges support by grants from the GIF, EU/FP7 via ERC grant 307260, ‘The Quantum Universe’, I-CORE programme by the Israeli Committee for planning and budgeting, the Kimmel award, and the Lord Sieff of Brimpton Fund. AVF’s group at UC Berkeley has received generous financial assistance from Gary and Cynthia Bengier, the Christopher R. Redlich Fund, the Richard and Rhoda Goldman Fund, the TABASGO Foundation, and NSF grant AST-1211916. JMS is supported by an NSF Astronomy and Astrophysics Postdoctoral Fellowship under award AST-1302771. EOO is incumbent of the Arye Dissentshik career development chair and is grateful to support by a grant from the Israeli Ministry of Science and the I-CORE programme of the Planning and Budgeting Committee and the Israel Science Foundation (grant No 1829/12).

We thank the very helpful staffs of the various observatories (Palomar, Lick, KNPO, TNG, Keck) at which data were obtained. The W. M. Keck Observatory is operated as a scientific partnership among the California Institute of Technology, the University of California, and NASA; it was made possible by the generous financial support of the W. M. Keck Foundation. M. T. Kandrashoff and J. Rex assisted with the Lick observations. We are grateful to the following contributors to the IPN for support and sharing their data: I. G. Mitrofanov, D. Golovin, M. L. Litvak, A. B. Sanin, C. Fellows, K. Harshman, and R. Starr (for the Odyssey team), R. Aptekar, E. Mazets, V. Pal’shin, D. Frederiks, and D. Svinin (for the Konus-Wind team), A. von Kienlin and A. Rau (for the INTEGRAL team), T. Takahashi, M. Ohno, Y. Hanabata, Y. Fukazawa, M. Tashiro, Y. Terada, T. Murakami, and K. Makishima (for the Suzaku team), T. Cline, J. Cummings, N. Gehrels, H. Krimm, and D. Palmer (for the Swift team), and V. Connaughton, M. S. Briggs, and C. Meegan (for the Fermi GBM team). KH acknowledges NASA support for the IPN under the following grants: NNX10AI23G (*Swift*), NNX09AV61G (*Suzaku*), NNX09AU03G (*Fermi*), and NNX09AR28G (*INTEGRAL*).

REFERENCES

- Arcavi I. et al., 2010, *ApJ*, 721, 777
- Arnett W. D., 1982, *ApJ*, 253, 785
- Berger E. et al., 2011, *ApJ*, 743, 204
- Bersier D. et al., 2006, *ApJ*, 643, 284
- Bufano F. et al., 2012, *ApJ*, 753, 67
- Cano Z. et al., 2011a, *MNRAS*, 413, 669
- Cano Z. et al., 2011b, *ApJ*, 740, 41
- Cardelli J. A., Clayton G. C., Mathis J. S., 1989, *ApJ*, 345, 245
- enko S. B. et al., 2006, *PASP*, 118, 1396
- enko S. B., Gal-Yam A., Kasliwal M. M., Stern D., Markey K., Alduena E., Alduena A., Kuo S., 2013, *GCN Circ.*, 14998

- Chornock R. et al., 2010, preprint ([arXiv:1004.2262](https://arxiv.org/abs/1004.2262))
- Cobb B. E., Bailyn C. D., van Dokkum P. G., Buxton M. M., Bloom J. S., 2004, *ApJ*, 608, L93
- Cobb B. E., Bailyn C. D., van Dokkum P. G., Natarajan P., 2006, *ApJ*, 645, L113
- Corsi A. et al., 2011, *ApJ*, 741, 76
- D'Elia V. et al., 2013, *GCN Circ.*, 15000
- Deng J., Tominaga N., Mazzali P. A., Maeda K., Nomoto K., 2005, 624, 898
- Drout M. R. et al., 2011, *ApJ*, 741, 97
- Ferrero P. et al., 2006, *A&A*, 457, 857
- Filippenko A. V., 1997, *ARA&A*, 35, 309
- Foley R. J. et al., 2003, *PASP*, 115, 1220
- Fukugita M., Ichikawa T., Gunn J. E., Doi M., Shimasaku K., Schneider D. P., 1996, *ApJ*, 111, 1748
- Gal-Yam A., Ofek E. O., Shemmer O., 2002, *MNRAS*, 332, L73
- Gal-Yam A. et al., 2004, *ApJ*, 609, L59
- Gal-Yam A. et al., 2011, *ApJ*, 736, 159
- Galama T. J. et al., 1998, *Nature*, 395, 670
- Galama T. J. et al., 1999, *A&AS*, 138, 465
- Gaskell C. M., Cappellaro E., Dinerstein H. L., Garnett D. R., Harkness R. P., Wheeler J. C., 1986, *ApJ*, 306, L77
- Hjorth J. et al., 2003, *Nature*, 423, 847
- Humason M. L., Mayall N. U., Sandage A. R., 1956, *AJ*, 61, 97
- Iwamoto K. et al., 2000, *ApJ*, 534, 660
- Jin Z.-P. et al., 2013, *ApJ*, 774, 114
- Jordi K., Grebel E. K., Ammon K., 2006, *A&A*, 460, 339
- Law N. M. et al., 2009, *PASP*, 121, 1395
- Levan A. J. et al., 2013, preprint ([arXiv:1307.5338](https://arxiv.org/abs/1307.5338))
- Li W. et al., 2011, *MNRAS*, 412, 1441
- Malesani D. et al., 2004, *ApJ*, 609, L5
- Matheson T. et al., 2003, *ApJ*, 599, 394
- Mazzali P. A., Iwamoto K., Nomoto K., 2000, *ApJ*, 545, 407
- Mazzali P. A., Nomoto K., Patat F., Maeda K., 2001, *ApJ*, 559, 1047
- Mazzali P. A. et al., 2002, *ApJ*, 572, L61
- Mazzali P. A. et al., 2003, *ApJ*, 599, L95
- Mazzali P. A. et al., 2006a, *Nature*, 442, 1018
- Mazzali P. A. et al., 2006b, *ApJ*, 645, 1323
- Mazzali P. A. et al., 2008, *Science*, 321, 1185
- Mazzali P. A., Walker E. S., Pian E., Tanaka M., Corsi A., Hattori T., Gal-Yam A., 2013, *MNRAS*, 432, 2463
- Melandri A. et al., 2012, *A&A*, 547, A82
- Milisavljevic D. et al., 2013, *ApJ*, 770, L38
- Mirabal N., Halpern J. P., An D., Thorstensen J. R., Terndrup D. M., 2006, *ApJ*, 643, L99
- Modjaz M. et al., 2006, *ApJ*, 645, L21
- Nakamura T., Mazzali P. A., Nomoto K., Iwamoto K., 2001, *ApJ*, 550, 991
- Nomoto K., Iwamoto K., Suzuki T., 1995, *Phys. Rep.*, 256, 173
- Ofek E. O. et al., 2012, *PASP*, 124, 62
- Olivares E. et al., 2012, *A&A*, 539, A76
- Patat F. et al., 2001, *ApJ*, 555, 900
- Pian E. et al., 2006, *Nature*, 442, 1011
- Pignata G. et al., 2011, *ApJ*, 728, 14
- Podsiadlowski P., Joss P. C., Hsu J. J. L., 1992, *ApJ*, 391, 246
- Podsiadlowski P., Mazzali P. A., Nomoto K., Lazzati D., Cappellaro E., 2004, *ApJ*, 607, L17
- Poznanski D., Ganeshaligam M., Silverman J. M., Filippenko A. V., 2011, *MNRAS*, 415, L81
- Poznanski D., Prochaska J. X., Bloom J. S., 2012, *MNRAS*, 426, 1465
- Rahmer G., Smith R., Velur V., Hale D., Law N., Bui K., Petrie H., Dekany R., 2008, in McLean I. S., Casali M. M., eds, *Proc. SPIE*, Vol. 7014, *Ground-based and Airborne Instrumentation for Astronomy II*. SPIE, Bellingham
- Rau A. et al., 2009, *PASP*, 121, 1334
- Sahu D. K., Tanaka M., Anupama G. C., Gurugubelli U. K., Nomoto K., 2009, *ApJ*, 697, 676
- Sanders N. E. et al., 2012, *ApJ*, 756, 184
- Schlegel D. J., Finkbeiner D. P., Davis M., 1998, *ApJ*, 500, 525
- Schulze S., Leloudas G., Xu D., Fynbo J. P. U., Geier S., Jakobsson P., 2013, *GCN Circ.*, 14994
- Singer L. P. et al., 2013, *ApJ*, 776, L34
- Smartt S. J., 2009, *ARA&A*, 47, 63
- Smartt S. J., Eldridge J. J., Crockett R. M., Maund J. R., 2009, *MNRAS*, 395, 1409
- Soderberg A. M. et al., 2005, *ApJ*, 627, 877
- Soderberg A. M., Chevalier R. A., Kulkarni S. R., Frail D. A., 2006, *ApJ*, 651, 1005
- Sollerman J. et al., 2006, *A&A*, 454, 503
- Sparre M. et al., 2011, *ApJ*, 735, L24
- Stanek K. Z. et al., 2003, *ApJ*, 591, L17
- Starling R. L. C. et al., 2011, *MNRAS*, 411, 2792
- Sugimoto D., Nomoto K., 1980, *Space Sci. Rev.*, 25
- Taubenberger S. et al., 2006, *MNRAS*, 371, 1459
- Thomsen B. et al., 2004, *A&A*, 419, L21
- Turatto M., Benetti S., Cappellaro E., 2003, in Hillebrandt W., Leibundgut B., eds, *ESO Astrophysics Symposia, From Twilight to Highlight: The Physics of Supernovae*. Springer-Verlag, Berlin, p. 200
- Valenti S. et al., 2007, *MNRAS*, 383, 1485
- Xu D. et al., 2013, *ApJ*, 776, 98
- Yaron O., Gal-Yam A., 2012, *PASP*, 124, 668
- Young D. R. et al., 2010, *A&A*, 512, A70

This paper has been typeset from a $\text{\TeX}/\text{\LaTeX}$ file prepared by the author.